A New Quantification Method of Bacterial Adherence on Implant Surfaces in an Implant Associated Infection Rat Model

Schröder ML[1,2], Angrisani N[2*], Hegermann J[3], Windhagen H[4], Calließ T[4] and Reifenrath J[2]

[1]University of Veterinary Medicine Hannover, Foundation, Small Animal Clinic, Bünteweg 9, Hannover, Germany

[2]Hannover Medical School, Clinic for Orthopedic Surgery, NIFE-Lower Saxony Centre for Biomedical Engineering, Implant Research and Development, Stadtfelddamm, Hannover, Germany

[3]Hannover Medical School, Institute of Functional an Applied Anatomy, Core-Unit Electron Microscopy, Carl-Neuberg, Hannover, Germany

[4]Hannover Medical School, Clinic for Orthopedic Surgery, Anna-von-Borries, Hannover, Germany

*Corresponding author: Nina Angrisani, Hannover Medical School, Clinic for Orthopedic Surgery/ NIFE Stadtfelddamm 34, 30625 Hannover, Germany, Tel: + 495115328961; Fax: +495115328314; E-mail: angrisani.nina@mh-hannover.de

Abstract

Objective: Implant infections in elective orthopedic surgery are still a clinically relevant problem with devastating consequences for the patient. Thereof results a great need for new strategies to prevent implant infections. Functionalization of implant surfaces to reduce the microbial adherence show great potential *in vitro*, but have to be tested in suitable models *in vivo*. Proper evaluation methods of the bacterial load on the implant surface are important for their evaluation. Up to now, the simultaneous assessment of the quantity and morphology of the bacterial infection *in vivo* was not performed.

Methods: Cubic Ti90/Al6/V4-rods were inserted in the tibia of Lewis rats and infected with *Staphylococcus aureus* strain 36/07 in different concentrations. After 21 days, explanted implants were stained for living and dead cells. The bacterial surface colonization was analyzed by confocal microscopy and assessed semi quantitatively via two different approaches (spot method and volume method) using the software Imaris ×64. Furthermore the bacterial morphology was evaluated. The results were compared to radiographic and histological changes.

Results: The new semi quantitative CLSM evaluation to assess the bacterial biomass on implant surfaces was successfully implemented. Both methods gave equivalent results. The results of the morphologic assessment of the bacterial colonization were similar to those of the quantification. A tendency towards increasing bacterial biomass and biofilm formation on the implant surface was observed with decreasing infection concentrations. In contrast, histologic and radiographic assessment as well as the relative tibial bone weight revealed more severe changes for higher inoculation concentrations.

Conclusion: In combination with the morphological assessment of the bacterial appearance this CLSM based evaluation is a suitable tool to assess the bacterial load on the implant surface. Combined with radiographical and histological evaluation of bone alterations, this model is appropriate for the evaluation of new implant surfaces.

Introduction

Implant infection is one of the most challenging complications in orthopedic surgery because of the devastating consequences for the patients including a prolonged hospital stay, pain, immobilization, multiple surgeries and antibiotic therapy [1-5]. Infection rates range from 0.5% to 7.5% in elective arthroplasty surgery [6-10] and from 0.5% up to 20% in acute trauma surgery [11,12]. The incidence depends mostly on the surgical complexity and patient related risk factors like diabetes or contaminated open fractures [12,13].

Increasing numbers of antimicrobiological resistances of bacteria complicate the use of antibiotics in the therapy of implant associated infections [14,15]. Many relevant pathogens have the ability to form biofilms [13,16], which enable the pathogens to grow less susceptible or resistant against antibiotic therapy and therefore turn into a persistent infection [17]. Therefore, the therapeutic intervention especially of low grade implant associated infections is challenging [14,18].

To prevent implant infections or at least reduce their formation beforehand, much research is performed on antibacterial implant surfaces [19-21]. However, the development of the ideal antibacterial implant surface is very challenging, because these surfaces have to prevent bacterial adhesion while simultaneously keeping adequate biocompatibility and promoting osseointegration [19,22]. Surface modification is one approach for antibacterial implant surfaces and has shown a bacterial repellent effect *in vitro* [23]. To test nano and micro structures *in vivo*, suitable animal models and evaluation techniques need to be available.

Existing strategies aim to quantify the bacterial colonialization on the implant surface by the use of sonication and afterwards counting of colony forming unit (CFU) or a morphological assessment of the

bacterial colonization on the implant surface via semi quantitative scoring schemata [24-28]. Nevertheless, the quantification is not precise in these models. Doll et al. compared confocal microscopic imaging via LIVE/DEAD staining on the implant surface to microbiologic methods (ultrasonic or enzymatic detachment with following CFU counting) to quantify the biofilm load on a defined titanium surface *in vitro* [29]. The detachment via sonication showed a lower number of CFU compared to enzymatic detachment and quantification via LIVE/DEAD staining. In the sonication process, the number of CFU is usually smaller than the proper bacterial load on the implant surface due to a higher amount of dead bacteria. Furthermore the sonication method cannot display the morphological features of biofilm formation attached to the implant surface. The differentiation of biofilm or planktonic bacteria by the use of LIVE/DEAD staining is much more simple than the differentiation of the morphology of planktonic and biofilm colonies on agar plates because of the diverse colony morphology as shown in *in vitro* studies on *Pseudomonas aeruginosa* strains [30]. If planktonic and biofilm derived colonies can equally distinguished for *S. aureus* strain 36/07 has not been examined yet. Furthermore the colony morphology does only give quantitative information and no details about the actual biofilm morphology and the distribution on the implant surface.

Glage et al. used a semi quantitative scoring method to evaluate S. aureus infected screws in a neurosurgical infection model [25]. The morphologic state of the bacteria provides the basis for the scoring scheme with score values from 0 to 5 for scattered bacteria to the quantity of formed microcolonies and biofilm formation. This model is suitable for the plain proof of concept. To evaluate new bacterial repellent surfaces, a more accurate assessment is preferable, ideally combining a morphological and semiquantitative evaluation of the bacteria on the implant surface.

The aim of this study was to implement an implant associated osteomyelitis animal model and to establish a method for the comprehensive assessment of the bacterial growth on implants to test modified implant surfaces *in vivo* for their capacity to reduce bacterial colonization.

Materials and Methods

Implants, bacteria and preparation of inocula, animal experiments

As implant material, cubic Ti90/Al6/V4-rods were used (n=56, dimensions $0.8 \times 0.8 \times 12$ mm³). They were cut out of a 50×50 mm plate (Goodfellow GmbH, Germany) by water jet cutting in the Institute of Materials Science, Leibniz Universität Hannover, Germany. An additional polishing with a 45 μm diamond abrasive polishing wheel (Power ProTM 4000, Buehler GmbH, Germany) was performed. Surface roughness (Rz=0.880 ± 0.214 μm, Ra=0.127 ± 0.025 μm Rmax=0.923 ± 0.188 μm) were determined according to DIN ISO 4289 at the Institute of Production Engineering and Machine Tools, Leibniz Universität Hannover.

The *S. aureus* strain 36/07 [31] was used in the present study, which was proven to induce an implant associated osteomyelitis in a neurosurgical implant related rat model [25]. Cultures were stored at -80°C as glycerol stocks in 10 μl aliquots. Pre-cultivation of the bacteria was performed prior to each experiment to reach the stationary phase. Therefore 5 μl of the stock were plated on blood agar with 5% sheep blood (BD Bioscience, Germany) and incubated for 14 hours at 37°C and aerobe conditions. The bacterial suspension for the injection was prepared by diluting *S. aureus* colonies of the pre-cultured blood agar plate in sterile 0.9% saline (B Braun, Germany) and adjusting the optical density (OD) at 600 nm to the ODs displayed in Table 1. Before and after the *in vivo* experimental use of the bacterial suspension standard plate counting was performed [29]. CFUs are expressed as means before and after surgery.

Localization	Criteria	Severity			
		absent	**mild**	**moderate**	**severe**
Bone marrow	Polymorphnuclear granulocytes	0	2	4	6
	micro abscesses	0	2	4	6
	fibrosis	0	2	4	6
Cortex	destruction	0	2	4	6
	polymorphnuclear granulocytes and osteoclasts	0	2	4	6
	microabscesses	0	2	4	6
	fibrosis	0	2	4	6
Periosteal reaction	quantity	0	2	4	6
Subjective impression	alteration	0	2	4	6

Table 1: Score for the evaluation of the pathohistological alterations after infection and implantation of the Ti90/Al6/V4 rod.

Adult male Lewis rats (n=39, LEW/NHanZtm, Laboratory Animal Science, Hannover Medical School, Germany) with an average body weight (BW) of 358 ± 32 g were used. All animal experiments were approved by the Lower Saxony State Office for Consumer Protection and Food Safety with the registration number 33.12-42502-04-16/2186.

Animals were randomly assigned to the experimental groups. Each animal received one implant into the left tibia and 10 μl of a bacterial suspension with the concentrations of 10^3, 10^4, 10^5, 10^6 CFU/10 μl

(n=8 animals/group, except 10^5: n=7). The control group (n=8) received sterile 0.9% saline (B Braun, Germany) instead of the bacterial suspension.

All surgical procedures were performed under general anesthesia by intramuscular injection of fentanyle 0.02 mg/kg BW (Fentanyl®-JANSSEN, Janssen-Cilag GmbH, Germany), medetomidine 0.2 mg/kg BW (Domitor®, Pfizer Deutschland GmbH, Germany) and midazolame 1 mg/kg BW (Dormicum®, Hameln Pharma Plus GmbH, Germany). Animals received carprofene 5 mg/kg BW subcutaneously (Rimadyl®, Zoetis Schweiz GmbH, Switzerland) for pain management and Sterofundin® HEG-5, 9 ml/kg BW (B. Braun, Germany). The left hind leg was shaved, disinfected and the operation field was prepared with a sterile perforated foil (Mölnlycke®, Germany). After an approximately 7 mm incision at the medio- proximal tibia, the drilling hole was established with a 1 mm drilling head on the first third of the medial tibial site. A 20 G canula was used for verifying the accessibility of the intramedullary cavity prior to the injection of the bacterial inoculum and implant insertion. After implant insertion, the drilling hole was sealed with bone wax (Assut Europe S.p.A., Germany). The implantation site was rinsed with ProntoVet® (B. Braun, Germany) and sterile 0.9% saline. The fascia and the skin were closed with Vicryl 4-0 (Ethicon, Johnson and Johnson Medical GmbH, Germany). To antagonize the anesthesia, animals received atipamezole 0.05 mg/kg BW (Antisedan®, Zoetis Schweiz GmbH, Switzerland), flumazenile 0.2 mg/kg BW (Flumazenil-Hameln, Hameln Pharma Plus GmbH, Germany) and naloxone 0.12 mg/kg BW (Naloxone-Inresa, Inresa Arzneimittel GmbH, Germany) subcutaneously (Table 2).

Group	OD600	CFU/10µl
Control	0	0.9% saline
10^6	0.636 ± 0.0121	$2.09 \pm 0.818 \times 10^6$
10^5	0.064 ± 0.0003	$4.85 \pm 0.537 \times 10^5$
10^4	0.014 ± 0.0004	$2.49 \pm 0.804 \times 10^4$
10^3	0.003 ± 0.0016	$1.0 \pm 0.33 \times 10^3$

Table 2: ODs and results of the standard plate counting on the day of surgery. The CFUs/10 µl of the bacterial suspension are displayed as the mean of the CFUs before and after surgery.

Post-surgical follow up

Analgetic treatment was carried out with carprofene for 3 days post-surgery (5 mg/kg BW subcutaneously). Carprofene or tramadol (Tramal, 2.5 mg/100 ml drinking water, Grünethal GmbH, Stolberg, Germany) were applied at any later time point, if necessary. Clinical checkup was performed daily. Radiographical examination was performed directly, 14 days and 21 days post-surgery in two planes (medio-lateral and anterior- posterior) under general anesthesia with 2.5%-5% isoflurane (CP-Pharma, Germany). Radiologic evaluation was performed blinded by 3 different veterinarians. A semi quantitative scoring scheme according to An and Friedman was partially modified and used for the evaluation [32]. Three regions of interest, the drilling hole, the implantation site and the area distal to the implant were assessed separately for their periosteal reaction and osteolysis. The whole bone was evaluated for the following criteria: general impression, fracture and sequester formation. Scores ranged from 0 (absent), 1 (mild), 2 (moderate) to 3 (extreme/severe). Fracture and sequester formation were scored with 0 (absent) and 1 (present). The summed maximum score was 23.

Euthanasia and probe sampling

All animals were deeply anaesthetized via an intraperitoneal injection of 60-80 mg/kg BW ketamine (Ketamin 10%, WDT, Germany) and 7-12 mg/kg BW xylazine (Sedaxylan®, WDT, Germany) 21 days post-surgery and sacrificed by exsanguination. The tibia was dissected with a saw under aseptic conditions. The implant was removed with forceps. Swabs were taken from the entry site before opening of the bone, one implant site and the bone marrow and plated on blood agar plates for 48h incubation under aerobic conditions at 37°C.

Tibial bone weight was determined directly after explantation with a high resolution balance (Extend BD-ED 100, Satorius AG, Germany). The bone weight was displayed in percentage relative to the body weight on the day of sacrifice.

Confocal laser scanning microscopic evaluation

The implants with adhering bacteria and eukaryotic cells were washed twice in sterile PBS to remove loosely bound structures on the implant surface. Afterwards they were stained with the LIVE/DEAD™ BacLight™ Bacterial Viability Kit (Thermo Fisher Scientific, Germany) for 15 minutes in a dilution of 1:1000 in PBS of both stains [33] and then fixed in 2.5% glutardialdehyde (Carl Roth GmbH, Germany) in PBS.

The LIVE stain Syto® 9 intercalates with the nucleic acids of all cells and fluoresces green. Propidium iodide is the red fluorescent DEAD stain and infiltrates exclusively cells with impaired cell membranes. It has a higher affinity to bind nucleic acids compared to Syto® 9 and therefore propidium iodide replaces Syto® 9 in dead cells [34]. Because of a limited staining time and higher amounts of nucleic acids in eukaryotic cells, an incomplete replacement of Syto® 9 by propidium iodide can occur especially in eukaryotic cells and a simultaneous staining of the live and dead stain is the result. This double staining is referred as colocalisation and is presented as a yellow to orange fluorescence.

Imaging was performed at 630-fold magnification by confocal laser scanning microscopy (CLSM, Leica TCS SP2, Leica Microsystems, Germany) and the software LCS (Leica Microsystems, Germany). Microscopy evaluation was performed on defined sections ($\approx$ 30000 µm²/area for each section). Z-stacks were performed to display the entire bacterial and eukaryotic cellular colonization on the implant surface. A laser with the wavelength of 488 nm was used for the excitation of the dyes and the settings for the emission spectra were 500-545 nm for Syto® 9 and 590-680 nm for propidium iodide.

For the measurement of the living bacterial biomass on the implant surface, eukaryotic cellular fractions and colocalized bacteria had to be subtracted from the total measured living volume. The calculation can be described with the following formula:

$$Live_{bacteria} = Live_{total} - (Live_{eukaryotic\ cells} + Colocalisation_{bacteria})$$

For these calculations the software package Imaris ×64 version 8.4 (Bitplane AG, Switzerland) was used to reconstruct three dimensional images of the confocal laser microscopic data. For the three dimensional reconstruction each z-stack was separately loaded in the

programme. Depending on the colonization size, the z-stacks varied between 5 and 150 pictures (interval per picture 1 µm).

The stepwise calculation and depiction of the relevant fractions is shown in Figure 1. The first step (I) was to calculate the total volume of the living, dead and colocalized biomass per section (in µm^3/A) using the corresponding fluorescence canals as published by Doll et al. [23,29]. After determining the volume for these three fractions, the second step (II) was to distinguish between bacterial and euaryotic cellular biomass in the fractions total living biomass and total colocalized biomass. For this purpose two different methods were used: The volume method (a) and the spot method (b).
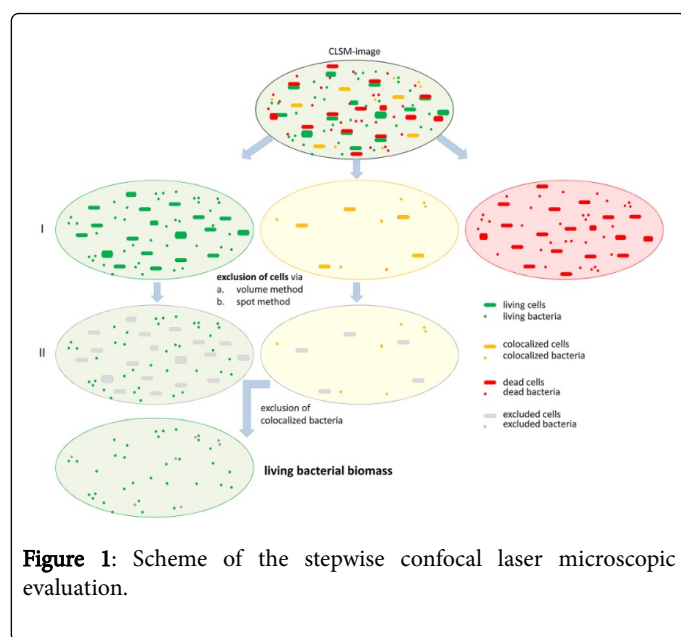
Figure 1: Scheme of the stepwise confocal laser microscopic evaluation.

Base values for both methods were determined using images of infected animals: The first parameter to distinguish between eukaryotic cells and bacteria was the size of the fluorescent structures. The second parameter was the fluorescence intensity. Compared to bacteria, eukaryotic cells have a higher amount of nucleic acids within the cell and therefore more binding sites for the stains. Hence, eukaryotic cells usually have higher fluorescence intensity.

For the volume method (a) the smallest detectable eukaryotic cell volume in these images was 10 µm^3. Therefore, green fluorescent structures on the surface of implants with a volume equal or larger than 10 µm^3 were included in the living eukaryotic cellular biomass (Live$_{eukaryotic\ cells}$) while yellow to orange fluorescent structures with a volume of 1-9 µm^3 were defined as colocalized bacteria (Colocalization$_{bacteria}$).

For the spot method (b) the diameter of approximately fifty eukaryotic cells in the images of infected animals were measured in two planes and averaged. This led to an average area of 5×6 µm^2 around which an oval shaped spot was formed. These oval shaped spots were placed into the green fluorescent structures on the surface of implants. Spots corresponding to the average area of 5×6 µm^2 or bigger were defined as living eukaryotic cellular biomass (Live$_{eukaryotic\ cells}$), while yellow to organge fluorescent structures which corresponded to oval shaped spots of 1×1 µm^2 were included in the colocalized bacterial biomass (Colocalization$_{bacteria}$).

Images, which had a total living biomass volume above 1.5×10^5 µm^3, were excluded because of an increased measurement error due to overlapping signal intensities of eukaryotic cellular and bacterial fractions. For each implant, a mean value of living bacterial biomass per section (in µm^3/A) was calculated.

Additionally, the living bacterial biomass on the implants was described morphologically by a score, which was adapted from the score of Glage et al. [25] (0=no bacteria on the implant surface, 1=scattered bacteria, 2=microcolonies, 3=commencing biofilm formation, 4=biofilm formation). Furthermore, extensive biofilm formation or the development of clusters in the extensive biofilm as well as the cell morphology were described.

Scanning electron microscopy

Exemplary colonized implants were scanned by SEM (Zeiss Crossbeam 540, Carl Zeiss Microscopy GmbH, Germany) after explantation and CLSM evaluation. Therefore, implants were fixed overnight in 150 mM Hepes, pH 7.35, containing 1.5% formaldehyde and 1.5% glutaraldehyde. After dehydration in acetone, implants were critical point dried and sputter coated with gold. Images were taken at 10 kV using a chamber SE-Detector.

Microcomputed tomographical examination

The residual tibiae were fixed in 3.5%-3.7% formaldehyde (Carl Roth GmbH and Co. KG, Germany) and exemplary µCT scans were performed (Inveon µCT, Siemens AG, Germany) at the imaging center for small animals at the Centre for Laboratory Animal Science, Hannover Medical School, Hannover. The scans were performed with a low system magnification using energy of 60 kV and an intensity of 500 µA. 720 projections were constructed with a 360° rotation.

Histological examination

After 2 days of fixation tibiae were divided at the middle of the implantation site by a diamond saw (Exakt, Helsinki, Finnland). The proximal part was decalcified for 18 days in a decalcification solution (USEDECALC®, Medite, Germany) and embedded in paraffin (Medite, Burgdorf), whereas the distal part was embedded in Technovit® 9100 Neu (Heraeus Kulzer GmbH, Germany) according to the protocol by Willbold and Witte [35]. Decalcified, paraffin embedded slices were stained using hematoxylin-eosin and Technovit® 9100 Neu embedded slices were stained using toluidine blue. Histological evaluation of the bone was done according to a modified semi quantitative score by Vogely et al. [36]. The bone marrow was evaluated for the quantity of polymorphnuclear granulocytes, microabscesses and fibrosis. The cortex was assessed for the severity of destruction and fibrotic conversion of the cortical bone as well as for the quantity of polymorphnuclear granulocytes, osteoclasts and microabscesses. The periosteum was evaluated for the severity of the reaction. Every slice was furthermore evaluated for its subjective impression of the pathohistological alterations. Higher values correspond to more severe histological changes; the maximum possible summed score was 54.
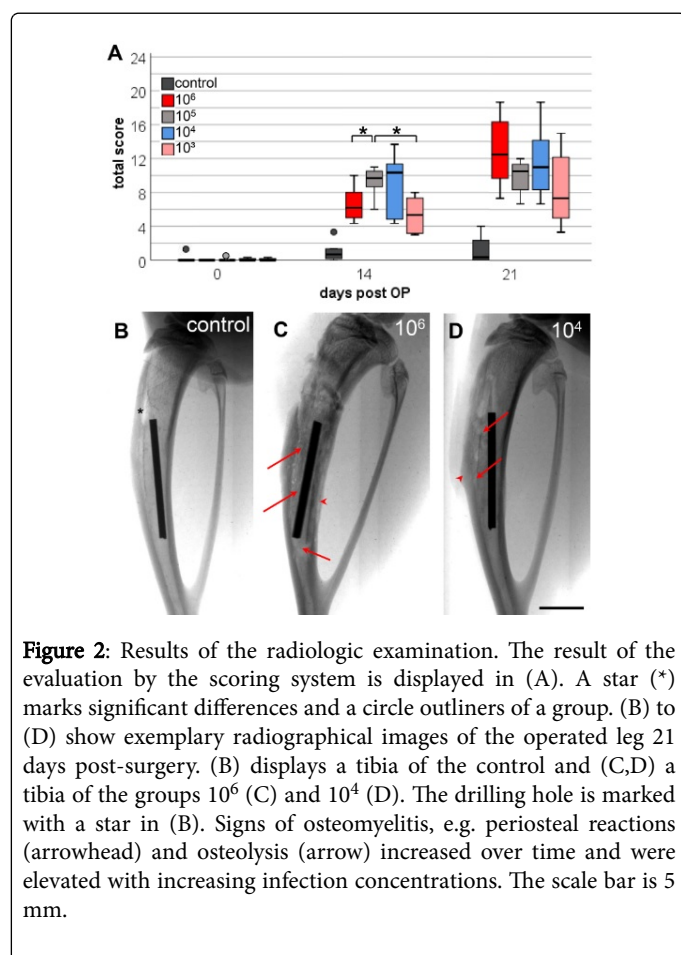
Statistical analysis

Statistical analysis was performed with SPSS 25 (IBM Deutschland GmbH, Germany). Data are expressed as means ± standard error (SE) for Gaussian distribution and medians (minimum/maximum) for non-Gaussian distribution. After testing for normal Gaussian distribution,

parametric, respectively non-parametric tests for significance were conducted. To test for differences within the groups for scores and non-parametric data, Friedmann test in combination with Wilcoxon test were used. For the detection of differences between the groups Kruskal-Wallis test in combination with the Man-Whitney-U test were used. One-way ANOVA was performed to test for significant differences in the relative tibial weight change. A p-value ≤ 0.05 was considered as statistically significant.

Results

Drop outs and injection concentrations

Two animal had to be excluded because of problems, which were not associated with the infection and two because of fracture of tibia or fibula; one animal each in groups 10^5 and 10^4. One animal in the group 10^6 died two days after surgery for no apparent reason. The concentrations of the bacterial injection suspension matched the aimed injection concentration.

Figure 2: Results of the radiologic examination. The result of the evaluation by the scoring system is displayed in (A). A star (*) marks significant differences and a circle outliners of a group. (B) to (D) show exemplary radiographical images of the operated leg 21 days post-surgery. (B) displays a tibia of the control and (C,D) a tibia of the groups 10^6 (C) and 10^4 (D). The drilling hole is marked with a star in (B). Signs of osteomyelitis, e.g. periosteal reactions (arrowhead) and osteolysis (arrow) increased over time and were elevated with increasing infection concentrations. The scale bar is 5 mm.

Post-surgical follow up

No significant changes could be detected between the groups in the daily clinical checkup. Three to four days after surgery, the gait normalized in all groups. In the group 10^6 two animals, in the group 10^5 one animal and in the group 10^4 one animal showed enhanced lameness of the operated leg, which decreased after analgesic treatment

with carprofene. One animal in the group 10^6 developed a bacterial knee infection.

Radiographical evaluation

Analysis of the radiographical evaluation on day 14 and 21 showed significantly increased score values compared to day 0 in all groups and a tendency of increased score values with increasing infection concentration (Figure 2). A significant increase in the score points at day 21 compared to day 14 was identified in the groups 10^6 and 10^3. A significant difference between the groups was determined on day 14 comparing the group 10^6 to the group 10^5 and the group 10^5 to the group 10^3.

Relative tibial weight and μCT examination

Figure 3 sums up the results of the tibial weight and the μCT evaluation.

Considering the relative tibial weight a decreasing tendency could be detected with decreasing infection concentrations. μCT examination showed morphological alterations in all examined bones. A beginning osseous incorporation of the implant could be detected by a complete or piecewise bony ring in the medullary cavity in the controls and in the vast majority of animals in the infected groups 10^5, 10^4 and 10^3. With increasing infection concentrations, an increasing osteolysis, a modification of the original bone by connecting tissue and periosteal reactions could be detected (Figure 3).

Microbiological examination

In the microbiological examination *S. aureus* 36/07 could not be detected in the control group in any smear of one implant site, the bone marrow or the implantation site. In four out of 8 animals small white colonies without haemolysis grew on the blood agar plates of the implantation site. They were analyzed by sequencing as contamination.

All animals in the infected groups showed a positive swab result for *S. aureus* in the bone marrow and on the implant. The smears of the implantation site of the infection groups were positive except for two cases: One in the group 10^5 and 10^3, respectively. One animal in the group 10^6 showed a positive result for *S. aureus* in the knee smear.

CLSM evaluation

The volume and the spot method showed similar results in the groups 10^6, 10^5, 10^4. However, in the control group and in the group 10^3 a significant difference in the median living bacterial biomass was determined comparing both methods (Figure 4).

Regarding the living bacterial biomass on the implant surface, no significant increase in the infected group 10^6 could be detected compared to the control. A significant increase in the living bacterial biomass could be determined in the groups 10^5, 10^4 and 10^3 compared to the control independent of the volume or spot method. Therefore a trend towards an increasing living bacterial biomass with decreasing infection concentrations could be observed.

The morphological evaluation of the implant surface showed eukaryotic cells on the implant surface of the control group, but no bacteria. But on the implant surface, roundly shaped eukaryotic cellular structures could be detected, which were larger than bacteria, but smaller than 10 μm³. All infection groups showed a significant difference compared to the control group. In the group 10^6 the

bacterial colonization showed a median score of 1 (1/3) with scattered bacteria on the implant surface and a few microcolonies. The group 10^5 had a median score of 1 (1/3), but showed an increased score of 2 and 3 on some images. An increased median score of 2 (1/4) and 2 (1/4) could be detected in the infected groups 10^4 and 10^3. The variation in these groups was higher, ranging from scattered bacteria to extensive biofilm formation on the implant surface. In the group 10^3 not only extensive biofilm formation could be detected, but also cluster formation within the extensive biofilm. The variation within the group 10^3 was high and ranged from scattered to clustered biofilm formation.
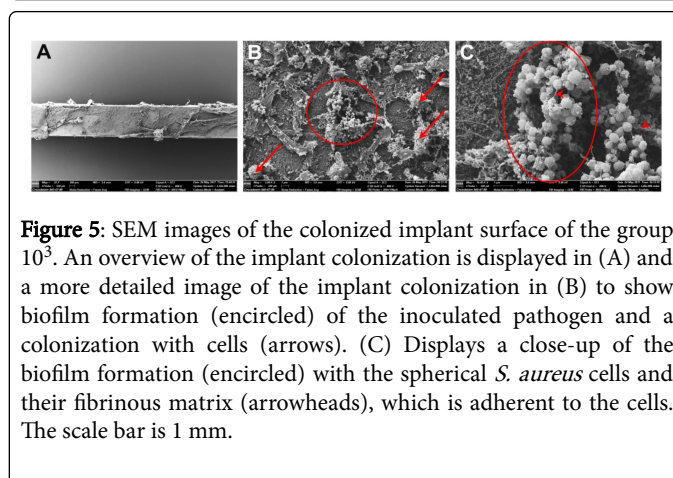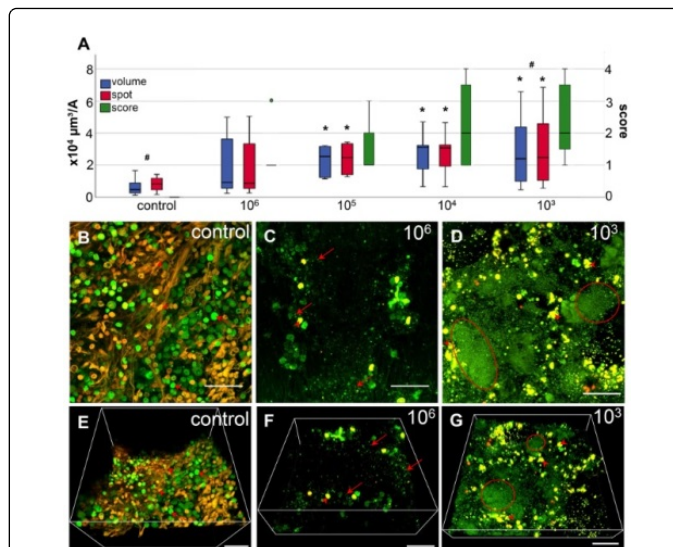
On all implant surfaces a variety of eukaryotic cells could be detected. Cells with a roundly shaped nucleus could be detected in all groups. The amount of cells with a polymorph nucleus was higher in all infected groups compared to in the control group. In all groups eukaryotic cells with extensions stained by the LIVE/DEAD dyes could be detected. These cells were more frequently seen in the control and the infected groups 10^5, 10^4 and 10^3. Cells with stained cytoplasm and more than one cell nucleus (usually 3 to 4 nuclei) were detected in all groups.

Figure 3: Relative tibial weight and corresponding morphological alterations of the tibia after 21 days. The infection-related alteration of the relative tibial weight is displayed in (A). A star (*) marks significant differences and a circle marks outliners of a group. Exemplary µCT cross sections of explanted tibiae are shown in (B-D). The control group is displayed in (B), 10^6 in (C) and 10^3 in (D). The former location of the implant is marked with a star (*). New bone formation is marked with arrowheads in (A) and (D). Decreasing bone alterations, e.g. osteolysis (encircled) and perisotal reactions (marked with an arrow) were observed with decreasing infection concentrations. The scale bar is 1 mm.
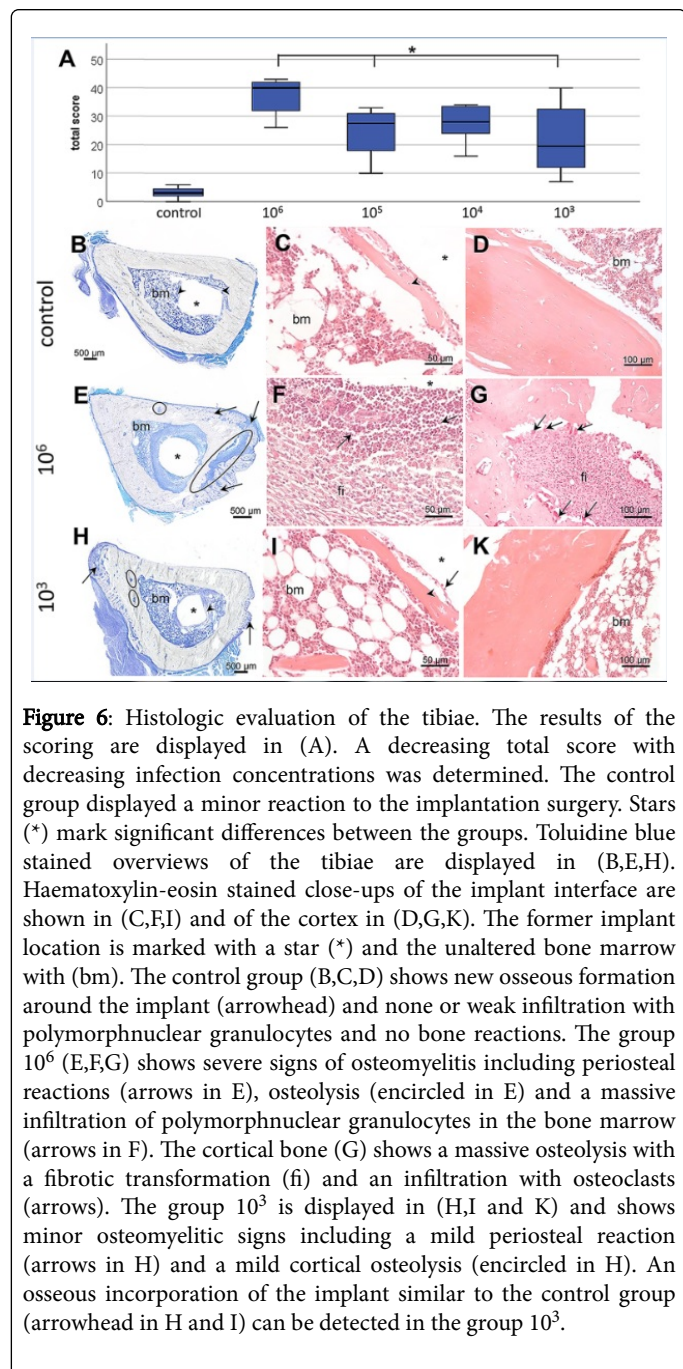
SEM examination

Exemplary SEM images revealed a colonization of the implant surface corresponding to the CLSM findings. In Figure 5 (A) an overview of the colonized implant surface is displayed. A close-up of the implant (Figure 5 (B)) shows the adherent eukaryotic cells as well as bacteria and their produced extracellular matrix. A detailed view of the biofilm formation of the infection pathogen is displayed in Figure 5 (C), where bacterial cell accumulation and the production of extracellular matrix were found.

Figure 4: CLSM evaluation of the bacterial colonization on the implant surface. (A) displays the results of the quantification of the living bacterial biomass using the Imaris® software package. The graph shows the volume/section (in μm^3/A) after subtraction of the living eucaryotic cell mass and the colocalized bacterial biomass by the volume method in blue and the spot method in red. The green bars display the results of the morphological scoring. Significant changes between the groups are marked with a star (*), differences between the evaluation methods with a hash (#) and outliners of a group with a circle. (B-G) show images of the same colonized implant surfaces in two (B-D) and three (E-G) dimensions. The images in (E,F) are rotated for a better presentation of the features. On the implant surface of the control animals (B,E), eukaryotic cells were observed with mostly round shaped nuclei (arrows) and with cellular extensions (arrowheads). The surface of the group 10^6 (C,F) shows mostly scattered bacteria (arrows) and eukaryotic cells with a polymorph nucelus (arrowhead). In contrast, on the implant surface of the group 10^3 (D,G), biofilm formation (encircled) and cells with a polymorph nucleus (arrowhead) could be detected. The scale bar is 40 µm.

Figure 5: SEM images of the colonized implant surface of the group 10^3. An overview of the implant colonization is displayed in (A) and a more detailed image of the implant colonization in (B) to show biofilm formation (encircled) of the inoculated pathogen and a colonization with cells (arrows). (C) Displays a close-up of the biofilm formation (encircled) with the spherical *S. aureus* cells and their fibrinous matrix (arrowheads), which is adherent to the cells. The scale bar is 1 mm.

Histological evaluation

The histological evaluation revealed the lowest summed score of 3 in the control group. The scores of the infection groups were all significantly elevated compared to the control. Furthermore significantly higher scores values could be detected for the group 10^6 compared to the groups 10^5 and 10^3 (Figure 6).

Figure 6: Histologic evaluation of the tibiae. The results of the scoring are displayed in (A). A decreasing total score with decreasing infection concentrations was determined. The control group displayed a minor reaction to the implantation surgery. Stars (*) mark significant differences between the groups. Toluidine blue stained overviews of the tibiae are displayed in (B,E,H). Haematoxylin-eosin stained close-ups of the implant interface are shown in (C,F,I) and of the cortex in (D,G,K). The former implant location is marked with a star (*) and the unaltered bone marrow with (bm). The control group (B,C,D) shows new osseous formation around the implant (arrowhead) and none or weak infiltration with polymorphnuclear granulocytes and no bone reactions. The group 10^6 (E,F,G) shows severe signs of osteomyelitis including periosteal reactions (arrows in E), osteolysis (encircled in E) and a massive infiltration of polymorphnuclear granulocytes in the bone marrow (arrows in F). The cortical bone (G) shows a massive osteolysis with a fibrotic transformation (fi) and an infiltration with osteoclasts (arrows). The group 10^3 is displayed in (H,I and K) and shows minor osteomyelitic signs including a mild periosteal reaction (arrows in H) and a mild cortical osteolysis (encircled in H). An osseous incorporation of the implant similar to the control group (arrowhead in H and I) can be detected in the group 10^3.

Discussion

For the analysis of the bacterial colonization on implant surfaces most studies used sonication and following CFU counting as a standard procedure [24,27,28,37]. Nevertheless *in vitro* experiments showed that the number of bacteria is lower compared to the quantification by LIVE/DEAD staining and CLSM [29]. The reason for this result is a higher amount of dead bacteria due to the sonication process. CFU counting after sonication only allows the quantification of colony forming bacteria, but does not take into account the morphological structure of the formed biofilm on the implant surface. The focus of this study was the assessment of the specific bacterial colonization on titanium implants including both quantity and morphology. With regard to the published *in vitro* results of Doll et al. [23] and the 3-R principles by Russel and Burch [38], especially the reduction of animal experiments, in the present study the comparison of CLSM examination with CFU counting was omitted.

Two different semiquantitative CLSM-based evaluation methods were tested and combined with a qualitative CLSM-based method for the morphological assessment of the bacterial appaerence on the implant surface. The primary objective of both quantitative methods (volume *vs.* spot) was the determination of the living bacterial biomass (in μm^3/A). Both methods were generally applicable. In the infected groups, the quantification of the biomass per section revealed a tendency towards an increased biomass with decreasing infection concentrations although not statistically significant. The most probable factor for the missing significance might be individual differences within the groups, which caused high standard deviations. These differences may be a result of different colonization within the animals and/or of the manipulation process during the pull-out, where tissue structures can tear of individually.

While the fluorescence intensity is equally regarded in both methods, the main difference is based on the critera to distinguish between cells and bacteria. In the volume method a certain volume (10 μm^3) was determined from which on structures were attributed to the cellular fraction. All structures smaller than this threshold value were attributed to the bacterial fraction. The main assumed advantage of this method was the higher accuracy since the whole cells including extensions were included in the cellular biomass. In contrast, the average two-dimensional diameter of eukaryotic cells (5×6 μm^2) and bacteria (1 μm^2) were determined for the spot method with a clear distance in between. Here it was hypothesized that the results should be more homogeneous with lower variances due to a more standardized calculation principle. Overall, there were no differences regarding the results of both methods, except for two groups with significant differences between volume and spot method (control and 10^3). In both groups the spot method led to a higher amount of living bacterial biomass than the volume method. To what extend the determined higher biomass in both groups influences the two methods differently is not yet known and possible reasons remain to be examined. Additionally it is noteworthy, that both methods showed bacterial biomass also in the control group. This result may be caused by background signals which corresponded to the signal of bacterial colonization. Actually, attribution to the bacterial biomass can be excluded due to negative swab results for all control implants and a negative result in the morphological evaluation. Therefore they are likely fragments of eukaryotic cells which were attributed to the bacterial biomass due to their size. However, the corresponding value determined by the volume method is lower than in the spot method. Due to this and the higher accuracy with simultaneously equivalent results the volume method should be favoured in future work.

For a more detailed evaluation of the biofilm forming capacity of the inoculated *S. aureus* strain, a morphological score adapted from Glage et al. [25] was used. While, contrary to our orthopedic model,

they inserted a screw in the cranium of rats and infected the screw with a concentration of 10^7 CFU/10 µl *S. aureus* 36/07, the results were similar to our 10^6 group: In particular scattered bacteria were forund on the implant surface after three weeks of incubation. Also Jørgensen et al. examined the biofilm formation of different *S. aureus* strains. They used a mouse model and assessed two epifluorescent *S. aureus* strains in the concentration of 10^4 CFU [28]. Epifluorescence microscopy and CLSM confirmed biofilm formation on the implanted steel pins with heterogenous distribution among the implants corresponding to our results with an infection concentration of 10^4.

The new evaluation method of the bacterial load on the implant surface has its limitations and has to be considered as semi quantitative, since images with a very dense colonization higher than 1.5×10^5 µm³/section had to be excluded from the evaluation due to overlapping fluorescence signals of cellular and bacterial structures. Additionally, the complexicity and duration of the CLSM examinations allow only for the evaluation of exemplary sections. However, it allows for a simultaneous evaluation of both the quantitative bacterial load and the morphological state of the biofilm. Because of the problems arising with the formation of biofilm on surgical implants in clinical situations, this combination of quantitative and morphologic evaluation for the differentiation of planktonic and biofilm forming bacteria is very important [39,40].

To further enhance the assessment an evaluation of radiographical, µ-computertomographical and histological changes can be added. Comparing the evaluation methods, radiologic and histological findings as well as the tibial weight showed similar results with regard to the severity of the implant associated osteomyelitis; values decreased with decreasing infection concentrations. These findings correspond to different other studies e.g. by Lucke et al. who modelled and implant associated osteomyelitis in the rat tibia [24] or Fukushima et al. who assessed the severity of an acute *S. aureus* (strain BB) induced osteomyelitis in the rat tibia without implant [37]. Although the assessment of the bacterial load provides important information about the state of the implant and therewith therapeutic options and prospect of success, no statement on clinical situation is done. Therefore, radiographical, µ-computertomographical and histological examinations can add important information on the patient strain.

Overall, biofilm formation is more attributed to low infection concentrations and there with low grade implant infections, while high infection concetrations in this study (10^6) primarily mimic acute severe implant infections.

The increasing biofilm formation with decreasing inoculation concentration might be a result of an increased immunological response to the higher initial bacterial threat. Referring to the histologically detectable more severe bone alterations and increased infiltration of immune cells with higher bacterial concentrations, we hypothesize that this intensified immune reaction leads to a proinflammatory environment due to the activation of polymorphnuclear neutrophils and osteoclasts resulting in more severe bone alterations, while biofilm maturation is reduced [41,42]. Haenle et al. implanted a Ti90/Al6/V4 conical implant into the metaphysis of the tibia and infected with a *S. aureus* strain (ATCC 25923) in concentrations of 10^3 to 10^6 [27]. The CFU counts of the sonicated implant did not differ between the infected groups. In contrast to Haenle et al., Fukushima et al. detected decreasing CFU in the bone with increasing infection concentrations and thereby demonstrated a similar trend compared to our quantification of the bacterial biomass on the implant surface by LIVE/DEAD staining [37]. The question

remains to which extend the morphology and metabolic properties of the bacteria within the biofilm influences their colony forming capacities and therefore alter the determined quantities.

Conclusions

A method for the evaluation of biofilm formation on implants in an orthopedic rat model was developed which allows simultaneously a quantitative and morphological assessment. Both quantitative methods (volume and spot method) were applicable and led to similar results. The calculation by the volume method provided a more accurate determination of the living bacterial biomass compared to the spot method due to a lower false positive volume. Therefore further investigations should prefer the volume method. In combination with the morphological assessment of the bacterial colonization the CLSM based quantification is a suitable tool to evaluate the bacterial load on implant surfaces and their possible impact. Validity and evaluation of the results could be enhanced by combination with imaging techniques or histological findings.

Acknowledgements

References

1. Parvizi J, Adeli B, Zmistowski B, Restrepo C, Greenwald AS (2012) Management of periprosthetic joint infection: The current knowledge: AAOS exhibit selection. J Bone Joint Surg Am 94: e104.

2. Bozic KJ, Ries MD (2005) The impact of infection after total hip arthroplasty on hospital and surgeon resource utilization. J Bone Joint Surg Am 87: 1746-1751.

3. Strange S, Whitehouse MR, Beswick AD, Board T, Burston A, et al. (2016) One-stage or two-stage revision surgery for prosthetic hip joint infection. The INFORM trial: A study protocol for a randomised controlled trial. Trials 17: 90-97.

4. Aggarwal VK, Rasouli MR, Parvizi J (2013) Periprosthetic joint infection: Current concept. Indian J Orthop 47: 10-17.

5. Zimmerli W, Trampuz A, Ochsner PE (2004) Prosthetic-Joint Infections. New Engl J Med 351: 1645-1654.

6. Phillips JE, Crane TP, Noy M, Elliott TS, Grimer RJ (2006) The incidence of deep prosthetic infections in a specialist orthopaedic hospital: A 15-year prospective survey. J Bone Joint Surg Br 88: 943-948.

7. Dale H, Hallan G, Espehaug B, Havelin LI, et al. (2009) Increasing risk of revision due to deep infection after hip arthroplasty. Acta Orthop 80: 639-645.

8. Mortazavi SM, Schwartzenberger J, Austin MS, Purtill JJ, Parvizi J (2010) Revision total knee arthroplasty infection: Incidence and predictors. Clin Orthop Relat Res 468: 2052-2059.

9. Singh JA, Sperling JW, Schleck C, Harmsen WS, Cofield RH (2012) Periprosthetic infections after total shoulder arthroplasty: A 33-year perspective. J Shoulder Elbow Surg 21: 1534-1541.

10. Achermann Y, Vogt M, Spormann C, Kolling C, Remschmidt C, et al. (2011) Characteristics and outcome of 27 elbow periprosthetic joint infections: Results from a 14 year cohort study of 358 elbow prostheses. Clin Microbiol Infect 17: 432-438.

11. Trampuz A, Widmer AF (2006) Infections associated with orthopedic implants. Curr Opin Infect Dis 19: 349-356.

12. Hull PD, Johnson SC, Stephen DJ, Kreder HJ, Jenkinson RJ (2014) Delayed debridement of severe open fractures is associated with a higher rate of deep infection. Bone Joint J 96: 379-384.

13. Fernandes A, Dias M (2013) The microbiological profiles of infected prosthetic implants with an emphasis on the organisms which form biofilms. J Clin Diagn Res 7: 219-223.

14. Furustrand TU, Crvec S, Betrisey B, Zimmerli W, Trampuz A (2012) Role of rifampin against Propionibacterium acnes biofilm in vitro and in an experimental foreign-body infection model. Antimicrob Agents Chemother 56: 1885-1891.

15. Zajonz D, Wuthe L, Rodloff AC, Prietzel T, von Salis-Soglio GF, et al. (2016) Infections of hip and knee endoprostheses. Spectrum of pathogens and the role of multiresistant bacteria. Chirurg 87: 332-339.

16. Arciola CR, Campoccia D, Speziale P, Montanaro L, Costerton JW (2012) Biofilm formation in Staphylococcus implant infections. A review of molecular mechanisms and implications for biofilm-resistant materials. Biomaterials 33: 5967-5982.

17. Høiby N, Bjarnsholt T, Givskov M, Molin S, Ciofu O (2010) Antibiotic resistance of bacterial biofilms. Int J Antimicrob Agents 35: 322-332.

18. Bowler LL, Zhanel GG, Ball TB, Saward LL (2012) Mature Pseudomonas aeruginosa biofilms prevail compared to young biofilms in the presence of ceftazidime. Antimicrob Agents Chemother 56: 4976-4979.

19. Arciola CR, Campoccia D, Ravaioli S, Montanaro L (2015) Polysaccharide intercellular adhesin in biofilm: Structural and regulatory aspects. Front Cell Infect Microbiol 5: 7-16.

20. Raphel J, Holodniy M, Goodman SB, Heilshorn SC (2016) Multifunctional coatings to simultaneously promote osseointegration and prevent infection of orthopaedic implants. Biomaterials 84: 301-314.

21. Inzana JA, Schwarz EM, Kates SL, Awad HA (2016) Biomaterials approaches to treating implant-associated osteomyelitis. Biomaterials 81: 58-71.

22. Gristina AG (1987) Biomaterial-centered infection: Microbial adhesion versus tissue integration. Science 237: 1588-1595.

23. Doll K, Fadeevaa E, Stumpp NS, Grade S, Chichkov BN et al. (2016) Reduced bacterial adhesion on titanium surfaces micro-structured by ultra-short pulsed laser ablation. BioNanoMat 17: 53-57.

24. Lucke M, Schmidmaier G, Sadoni S, Wildemann B, Schiller R, et al. (2003) A new model of implant-related osteomyelitis in rats. J Biomed Mater Res B Appl Biomater 67: 593-602.

25. Glage S, Paret S, Winkel A, Stiesch M, Bleich A, et al. (2017) A new model for biofilm formation and inflammatory tissue reaction: Intraoperative infection of a cranial implant with Staphylococcus aureus in rats. Acta Neurochir (Wien) 159: 1747-1756.

26. Hoene A, Walschus U, Patrzyk M, Finke B, Lucke S, et al. (2010) In vivo investigation of the inflammatory response against allylamine plasma polymer coated titanium implants in a rat model. Acta Biomater 6: 676-683.

27. Haenle M, Zietz C, Lindner T, Arndt K, Vetter A, et al. (2013) A model of implant-associated infection in the tibial metaphysis of rats. Sci World J 2013: 1-8.

28. Jørgensen NP, Meyer RL, Dagnaes-Hansen F, Fuursted K, Petersen E (2014) A modified chronic infection model for testing treatment of Staphylococcus aureus biofilms on implants. PLoS One 9: e103688.

29. Doll K, Jongsthaphongpun KL, Stumpp NS, Winkel A, Stiesch M (2016) Quantifying implant-associated biofilms: Comparison of microscopic, microbiologic and biochemical methods. J Microbiol Methods 130: 61-68.

30. Sousa AM, Machado I, Nicolau A, Pereira MO (2013) Improvements on colony morphology identification towards bacterial profiling. J Microbiol Methods 95: 327-335.

31. Baraki H, Zinne N, Wedekind D, Meier M, Bleich A, et al. (2012) Magnetic resonance imaging of soft tissue infection with iron oxide labeled granulocytes in a rat model. PLoS One 7: e51770.

32. An YH, Friedman RJ (1998) Animal models of orthopedic implant infection. J Invest Surg 11: 139-146.

33. (2004) Molecular Probes. Product Information LIVE/DEAD® BacLightTM Viability Kits.

34. Stocks SM (2004) Mechanism and use of the commercially available viability stain, BacLight. Cytometry A 61: 189-195.

35. Willbold E, Witte F (2010) Histology and research at the hard tissue-implant interface using Technovit 9100 New embedding technique. Acta Biomater 6: 4447-4455.

36. Vogely HC, Oosterbos CJ, Puts EW, Nijhof MW, Nikkels PG, et al. (2000) Effects of hydrosyapatite coating on Ti-6Al-4V implant-site infection in a rabbit tibial model. J Orthop Res 18: 485-493.

37. Fukushima N, Yokoyama K, Sasahara T, Dobashi Y, Itoman M (2005) Establishment of rat model of acute staphylococcal osteomyelitis: relationship between inoculation dose and development of osteomyelitis. Arch Orthop Trauma Surg 125: 169-176.

38. Russell W.M.S., Burch R.L. (1959) The principles of humane experimental technique. (1st edtn). Methuen and Co. Ltd, London.

39. Penesyan A, Gillings M, Paulsen IT (2015) Antibiotic discovery: combatting bacterial resistance in cells and in biofilm communities. Molecules 20: 5286-5298.

40. Grau L, Gunder MA, Schneiderbauer M (2017) Difficult-to-detect low-grade infections responsible for poor outcomes in total knee arthroplasty. Am J Orthop (Belle Mead NJ) 46: e148-e153.

41. Dapunt U, Hännsch GM, Arciola CR (2016) Innate immune response in implant-associated infections: Neutrophils against biofilms. Materials (Basel) 9: E387-388.

42. Trouillet-Assant S, Gallet M, Nauroy P, Rasigade JP, Flammier S, et al. (2015) Dual impact of live Staphylococcus aureus on the osteoclast lineage, leading to increased bone resorption. J Infect Dis 211: 571-581.